ROYAL SOCIETY OF CHEMISTRY

ChemComm

COMMUNICATION

Construction of 2D g-C₃N₄ lateral-like homostructures and their photo- and electro-catalytic activities[†]

Xiao Zhang,[a] Jean-Pierre Veder,[b] Shuai He,[a] and San Ping Jiang*[a]

g-C₃N₄ crystalline/amorphous lateral-like homostructures were prepared using crystalline g-C₃N₄ nanosheets as seeds via sequential edge-epitaxy growth. The homojunction effectively separates photogenerated carriers, resulting in the high photo- and electro-catalytic activities.

Two-dimensional (2D) in-plane heterojunctions have attracted significant attentions because of their superior properties generated by electrons that are free to move but restricted in the third direction.[1] Such 2D heterostructures consisted of single or several atomic layers do not exist in nature, but can be fabricated through the epitaxial growth strategy. Currently, the study of 2D in-plane heterojunctions mainly focused on transition metal dichalcogenides (TMD) due to the nature of the heterostructures. For example, Chiu and co-workers reported on TMD artificial heterostructures prepared via a multistep chemical vapor deposition (CVD) synthesis.[1a] Duan's group fabricated 2D WS₂-WSe₂ heterostructures with precisely controlled spatial modulation.[1c] For other layered materials with covalent bonding (e.g. carbon based materials), the constructing of few-layer 2D lateral heterostructures becomes a challenge because of the limitation of structures.[2]

As a metal-free polymeric photocatalyst, graphic carbon nitride (g-C₃N₄) with a suitable bandgap energy of 2.7 eV for visible photocatalysis has attracted considerable attention compared with other 2D nanomaterials (e.g. graphene, MoS₂) because of its organic features.[3] g-C₃N₄ can be obtained by various methods, such as simultaneous exfoliation of bulk C₃N₄ into layers of C₃N₄ via mechanical grinding, chemical, and physical routes. The molecular structure and electronic properties of g-C₃N₄ could be easily modulated via forming

heterostructures, such as semiconductor phase growth, doping, and noble metal modification.[4] However, lateral heterostructures of g-C₃N₄ are rarely reported due to difficulties in synthesis. The heterostructure of g-C₃N₄ can be created via π-π stacking interactions, in which, vertical heterojunctions are achieved.[2a] Inversely, the unique in-plane 2D heterojunctions are obtained using direct CVD growth via edge epitaxy. It is facile to prepare TMD lateral heterostructures via CVD growth. Thus, a novel method with precise control is required for constructing g-C₃N₄ lateral-like heterostructures for high-efficiency photo- and electro-catalysts.

Herein, a multistep CVD method has been developed to prepare g-C₃N₄ crystalline/amorphous lateral-like homo-structures (Experimental, ESI†). Crystalline and amorphous g-C₃N₄ nanosheets were prepared via deposition and polymerization of melamine at different temperatures. Fig. 1
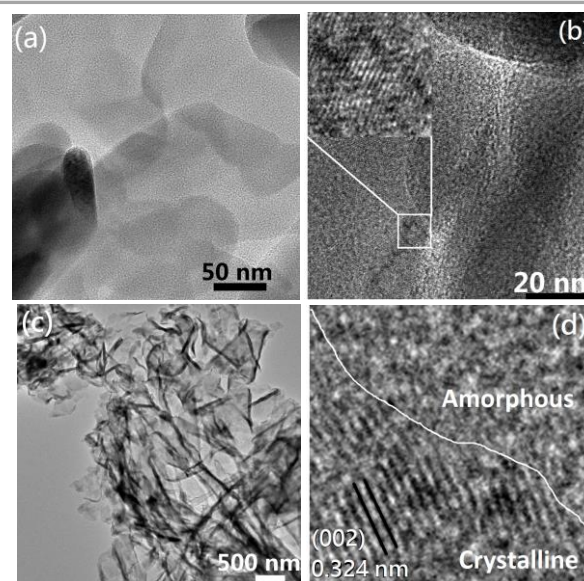
Fig. 1 TEM images of samples. (a) CN-650. (b) CN-750. (c) and (d) CN-750@650. The inset in (b) shows the lattice fringes of crystalline g-C₃N₄.

[a.] Fuels and Energy Technology Institute and Western Australia School of Mines: Minerals, Energy and Chemical Engineering, Curtin University, Perth WA6845, Australia. E-mail: S.Jiang@curtin.edu.au

[b.] John De Laeter Centre & Department of Physics and Astronomy, Curtin University, Perth, WA, 6102, Australia

shows the transmission electron microscopy (TEM) and high-resolution TEM images of g-C_3N_4 samples. The results indicate that sample prepared at 650 °C (CN-650) is amorphous (Fig. 1a) while sample prepared at 750 °C (CN-750) is crystalline (Fig. 1b). The crystallinity of CN-750 is ascribed to the slow multi-heating-treated procedure, multistep control, and high temperature setting. g-C_3N_4 crystalline/amorphous lateral-like homostructures were created using CN-750 as seed and prepared at 650 ºC (CN-750@650). CN-750@650 still remained a nanosheet morphology as shown in Fig. 1c. However, there clearly exist interfaces between the crystalline and amorphous g-C_3N_4 (Fig. 1d). The presence of defects in such crystalline/amorphous interfaces cannot be ruled out. The lattice fringes is 0.324 nm as (002) facet. Because of the crystallinity of CN-750, the edge-epitaxy growth of amorphous phase occurred. The interface of g-C_3N_4 crystalline/amorphous lateral-like homostructures is not like that of TMD in-plane heterostructures. The g-C_3N_4 crystalline/amorphous lateral-like homostructures consisted of few layers of g-C_3N_4.

X-ray diffraction (XRD) patterns of samples (Fig. S1, ESI†) indicate that two XRD peaks at 12.8° and 27.9° were observed for all three samples corresponding to the (100) and (002) facets, respectively. The weak peak is caused by the periodic arrangement of the triazine in g-C_3N_4 and the higher intensity peak is related to the stacking of the conjugated aromatic sections of carbon nitride.[5] All samples show g-C_3N_4 phase with identical XRD patterns. Nevertheless, the XRD peak intensity of CN-750 is the highest, suggesting that calcination at high temperature improves the crystallinity. The peak intensity of CN-750@650 is also enhanced compared with CN-650 due to the presence of crystalline g-C_3N_4 in the sample (Fig.1d).

Fig. 2a to 2f shows the X-ray photoelectron spectroscopy (XPS) spectra (e.g. C1s and N1s spectra) of CN-650, CN-750, and CN-750@650. The C1s spectra of samples show the peaks related C-C, C-O-C/C-OH, C=N, C-N, and satellite C1s peak (Fig. 2a, 2c and 2e). The peak intensity ratios are listed in Table S1 and S2 (ESI†). The N1s spectra of samples show the peak positions corresponding to C-N=C (Pyridinic-N), N-$(C)_3$ (Pyrrolic-N), N-H(graphitic N) (Fig. 2b, 2d and 2f). CN-650 shows high C-C and N-$(C)_3$ ratios as compared with CN-750, suggesting that the distillation of N element occurred at higher temperature. For the homostructure sample, the ratio of C-N peak is the highest. This could indicate the homojunction formation through the C-N connection. The N/C ratio of CN-650, CN-750, and CN-750@650 are 1.16, 0.90, and 1.17, respectively. This also confirms that the amount of N element decreased with increasing temperature. According to UV-VIS diffuse reflectance spectra, the band gap of the samples was estimated[6] by using the transformed Kubelka–Munk function (A(hv-Eg)r= α hv).[7] The band gaps of CN-650, CN-750, and CN-750@650 were estimated to be 2.55, 2.75, and 2.70eV, respectively (Fig, S2, ESI†). The band gap of CN-750@650 is between CN-650 and CN-750.
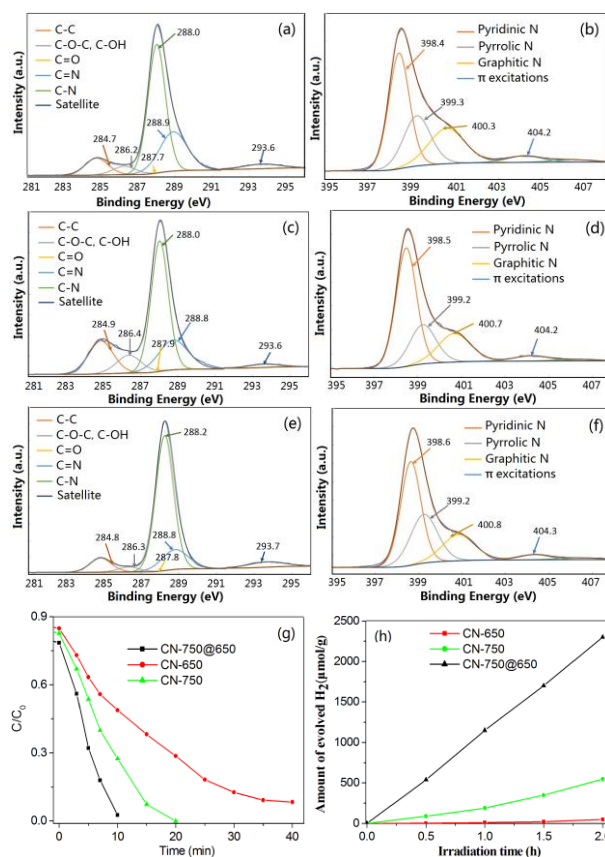

Fig. 2 XPS spectra (a to f) and Photocatalytic performance (g & h) of samples. (a, b) CN-650. (c, d) CN-750. (e, f) CN-750@650C. (g) Photocatalytic degradation plots of RhB with time and (h) H_2 production curves for H_2 evolution of samples under visible light (λ > 420 nm).

g-C_3N_4 is a typical material for photocatalyst under visible light.[8] The microstructure adjustment results in the change of photocatalytic activity. Fig. 2g shows the plots of rhodamine B (RhB) degradation under visible light. CN-750@650 revealed the fastest degradation, in which RhB was degraded completely within 10 min. In the case of CN-750, the degradation rate was half of that of the CN-750@650 sample. Moreover, only less than 50% of RhB was degraded after 10 min degradation using the CN-650 sample. The enhanced photocatalysis performance of CN-750@650 homostructures could be ascribed to the contribution of the possible defects in the interface between crystalline and amorphous phases which increases the active sites as well as the formation of lateral-like crystalline/ amorphous homojunctions which result in the effective separation of photogenerated carriers. This lateral-like homo-structure revealed quick degradation of RhB, as compared with layer-like g-C_3N_4 homo-structure.[2c] Furthermore, crystalline g-C_3N_4 has a better photocatalytic performance compared with the amorphous one. This could be ascribed to the change of composition and structure that provides more active sites. To confirm this, crystalline and amorphous g-C_3N_4 were mixed to check the photocatalysis performance. It was found that the photocatalysis performance of the mixed sample is only slightly better than that of the CN-650 sample. This confirms that g-C_3N_4

crystalline/amorphous homojunctions (CN-750@650) shows an obvious improvement in photocatalysis performance.

Fig. 2h show the H_2 evolution reaction (HER) for water splitting as a function of irradiation time. The amount of H_2 increased linearly with irradiation time. The efficiency of CN-750@650 is 46 times and 6 times high than that of the CN-650 and CN-750 samples, respectively. The reason for the enhanced photocatalytic performance of CN-750@650 can be discussed as follows. Both crystalline and amorphous g-C_3N_4 were formed through polymerization reaction.[9] The common characteristic of g-C_3N_4 photocatalyst is quick recombination of photogenerated electrons and holes, thus resulting in a low photocatalysis efficiency.[10a-b] Amorphous g-C_3N_4 was sequential edge-epitaxially grown on crystalline g-C_3N_4 to form the homostructures. Although the composition of two phases is similar, the change of crystallinity and N/C ratio (1.16 and 0.90 for CN-650 and CN-750, respectively) leads to changes in band gap of the samples. Thus, it is obvious that the homojunctions promote the spatial separation of electrons and holes and reduce the recombination rate. Stability test indicates the hydrogen generation and RhB degradation efficiencies of the homojunction sample remained almost unchanged after 5 cycles.

To improve electrochemistry property and to test charge transfer system, Pt was deposited on g-C_3N_4 using ultrasonic treatment and reduction by reflux. Fig. 3 shows the TEM, HRTEM, high-angle annular dark-field scanning TEM (HAADF-STEM) images and corresponding element mapping of Pt-deposited CN-750@650. The image in Fig. 3a shows the curvature on the edges of graphitic sheets after Pt deposition. Well-developed lattice fringes were observed (Fig.3b), but they do not match with that of the crystalline g-C_3N_4 and Pt. This is ascribed to the overlap of different crystal phases. During sonication treatment of water, reducing species (e.g. H atoms) could be generated within and/or at the interface of cavitation bubbles,[10c-e] which would result in the reduction of Pt ions. N, C, and Pt were found to be homogeneously distributed in the whole specimen area (Fig. 3c to 3f). The size of deposited Pt nanoparticles (NPs) was estimated to be in the range of 1-2 nm. However, the content of Pt is low. To increase the loading of Pt, reaction time was increased to 2h (Fig. S3 and S4, ESI†). The amount of Pt increased, but the distribution of Pt is still homogeneous, indicating the homogeneous Pt attachment on g-C_3N_4. The photocatalytic activity of Pt deposited samples was tested (Fig. S5, ESI†). Pt-deposited sample with short deposition time of 0.5 h revealed the best performance. After Pt modification, the performance of CN-650 and CN-750 were enhanced while that of the CN-750@650 sample decreased. This is ascribed to the fact that charge transfer in the homojunction was inhibited due to the electrons transfer to Pt. This further confirms the formation of the homostructures. The XPS analysis for Pt-modified CN-750 samples indicates the amount of Pt increased with time (Fig. S6, ESI ESI†).
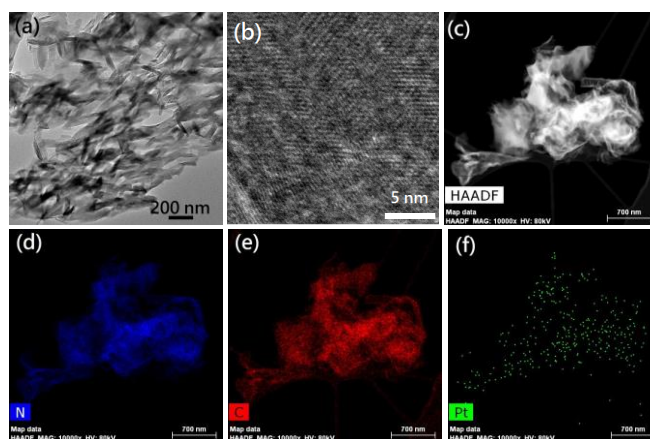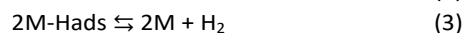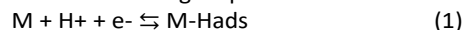

Fig. 3 (a) TEM, (b) HRTEM, (c) HAADF-STEM images and N (d), C (e), and Pt (f) mapping of Pt-deposited CN-750@650 with sonication for 0.5 h.

It is still a challenge to develop enhanced electrocatalytic HER using g-C_3N_4 with its unique electric, photo, and thermal effects.[11] Since g-C_3N_4 is commonly used as a photocatayst rather than an electrocatalyst, expanding in applications of g-C_3N_4 with its metal free and high stability properties need to be further explored. The HER polarization curves of g-C_3N_4 samples under visible light irradiation with a scan rate of 5 mV/s are shown in Fig. S7 (ESI†). As expected, crystalline CN-750 revealed the best performance even though the onset overpotential is not high. To obtain high efficient electrochemistry catalyst, Au was also deposited on CN-750. The electrocatalytic HER activities were investigated by linear sweep voltammetry (LSV) test. The HER polarization curves of CN-750 before and after Au or Pt modification are shown in Fig. 4a. It is clear that the Pt-modified samples have better HER
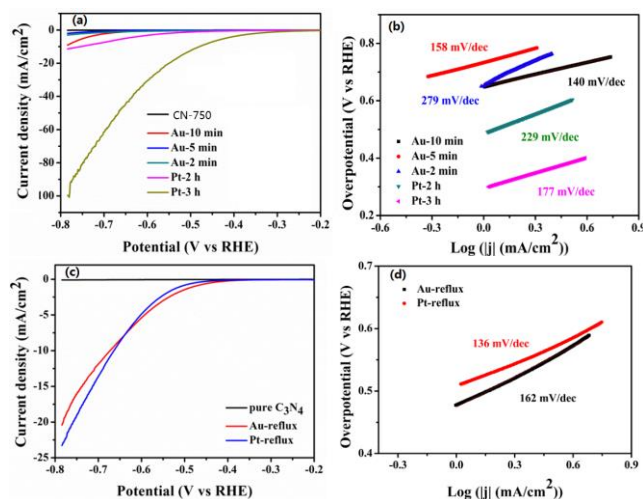
Fig. 4. (a) HER polarization curves of CN-750 before and after Au, Pt modification with different sonication time. (b) Tafel plots of the samples derived from HER polarization curves in (a). (c) HER polarization curves of CN-750 modification with Au and Pt by reflux. (d) Tafel plots of the samples derived from HER polarization curves in (c).

COMMUNICATION

activity than that of Au-modified ones due to the high intrinsic activity of Pt NPs, which reduces the hydrogen adsorption free energy. Pt deposited sample with reaction for 3h reveals the best performance. As the ultrasonic time increasing, the HER activity was improved, most likely due to the increased amount of small and uniform Pt NPs decorated on C_3N_4. The Tafel slopes were further used to characterize the reaction kinetic. The reaction pathway followed the Volmer-Heyrovsky mechanism, with the hydrogen adsorption reaction to be the rate-determining step.

$$M + H+ + e- \leftrightarrows M\text{-Hads} \qquad (1)$$
$$M\text{-Hads} + H+ + e- \leftrightarrows M + H_2 \qquad (2)$$
$$2M\text{-Hads} \leftrightarrows 2M + H_2 \qquad (3)$$

The HER activities of samples are assessed by Tafel slopes (Fig. 4b) which were calculated from the polarization curves according to the Tafel equation.[12]

As shown in Fig. 4a, the H_2 evolution performance of 3-hour Pt deposited CN-750 sample was significantly increased compared with other samples. This is ascribed to the fact that the increased amount of small and uniform Pt NPs was decorated on g-C_3N_4. The reaction was determined by Volmer step (Eq.1), and the values of Tafel slopes decreased, revealing the accelerated reaction kinetic. This result is different from the photocatalysis test. In that case, the sample with Pt reacted for 0.5 h revealed the best photocatalytic activity. This phenomenon is related to the difference of reaction mechanism for photocatalysis and electrocatalysis. For comparison, Au and Pt NPs were deposited using $NaHBO_4$ as reflux. The HER performance of Au-reflux and Pt-reflux samples is shown in Fig. 4c and 4d. The result indicates that the HER performance is not as good as that obtained on the Pt deposited sample with sonication for 3h. This is ascribed that the sizes of Au and Pt NPs are large and not homogeneous for samples obtained by reflux. Therefore, sonication is a sufficient way to form fine microstructure with superior electrochemistry activity.

In conclusion, a multistep CVD method has been developed to create g-C_3N_4 amorphous/crystalline homostructures. Amorphous and crystalline g-C_3N_4 were prepared at 650 and 750 °C, respectively. Using crystalline g-C_3N_4 as seeds, the amorphous/crystalline homostructures were edge-epitaxy grown at 650 °C via controlling the procedure. The homostructures reveals high photocatalysis and H_2 generation activity. In addition, Au and Pt NPs were deposited via a sonication method for the first time. After Au and Pt deposition, the performances are significantly enhanced. However, samples with different amount of Pt loading reveals different effect for the photocatalysis and elctrocatalysis performances. According to the unique microstructure and enhanced properties, these amorphous/crystalline homostructures and Pt modified materials would be of significant importance for electrocatalysis and photocatalysis applications.

Conflicts of interest

There are no conflicts to declare.

Notes and references

1 (a) K-C. Chiu, K-H. Huang, C-A. Chen, Y-Y. Lai, X-Q Zhang, E-C. Lin, M-H. Chuang, J-M. Wu, and Y-H. Lee, *Adv. Mater.* **2017**, 1704796. (b) P. K. Sahoo, S. Memaran, Y. Xin, L. Balicas, and H. R. Gutiérrez, *Nature*, 2018, **553**, 64. (c) Z. Zhang, P. Chen, X. Duan, K. Zang, J. Luo, and X. Duan, *Science*, 2017, **357**, 788. (d) C. Jia, X. Zhang, K. Matras-Postolek, B. Huang, and P. Yang, *Carbon*, 2018, **139**, 415. (e) Z. Jiang, X, Zhang, J. Wang, L. Chen, H. Chen, and P. Yang, *Chem. Commun.* 2018, **54**, 13519.

2 (a) J. Ji, J. Wen, Y. Shen, Y. Lv, Y. Chen, S. Liu, H. Ma, and Y. Zhang, *J. Am. Chem. Soc*. 2017, **139**, 11698. (b) X. Wang, K. Maeda, A. Thomas, K. Takanabe, G. Xin, J. M. Carlsson, K. Domen, M. Antonietti, *Nat. Mater*. 2009, **8**, 76. (c) Z. Liu, G. Wang, H-S. Chen, and P. Yang, *Chem. Commun*. 2018, **54**, 4720.

3 (a) J-T. Yin, Z. Li, Y. Cai, Q-F. Zhang, and W. Chen, *Chem. Commun*., 2017, **53**, 9430. (b) Y. Liu, X. Zhang, J. Wang, P. Yang, *Phys. Chem. Chem. Phys*., 2016. **18**. 31513

4 (a) L. Huang, Z. Liu, W. Chen, D. Cao, and A. Zheng, *J. Mater. Chem. A*, 2018, **6**, 7168. (b) Y. Wei, Z. Zhao, P. Yang, *ChemElectroChem*, 2018, **5**, 778. (c) F. Zhang, Q. Wen, M. Hong, Z. Zhuang, Y. Yu, *Chem. Eng. J.* 2017, **307**, 593. (d) M. Li, X. Zhang, K. Matras-Postolek, H-S. Chen, and P. Yang, *J. Mater Chem C*, 2018, **6**, 5506. (e) L. Shi, Z. Li, K. Marcus, G. Wang, K. Liang, W. Niua, and Y. Yang, *Chem. Commun*., 2018, **54**, 3747.

5 (a) F. He, G. Chen and Y. Yu, *Chem. Commun*., 2015, **51**, 6824. (b) Y. Hou, A. Laursen, J. Zhang, G. Zhang, Y. Zhu, X. Wang，S. Dahl and I. Chorkendorff, *Angew. Chem. Int. Ed.*, 2013, **52**, 3621.

6 (a) R. Ye, H. Fang, Y. Zheng, N. Li, Y. Wang, and X. Tao, *ACS Appl. Mater. Interfaces* 2016, **8**, 13879. (b) G. Zhang, A. Savateev, Y. Zhao, L. Li and M. Antonietti, *J. Mater. Chem. A,* 2017, **5**, 12723.

7 Q. Han, C. Hu, F. Zhao, Z. Zhang, N. Chen, L. Qu, *J. Mater. Chem. A*, 2015, **3**, 4612.

8 (a) X. Chen, W. Lu and T. Xu, *Chem. Eng. J.*, 2017, **328**, 853. (b) Y. Li, J. Zhang, Q. Wang, Y. Jin, D. Huang, Q. Cui, and G. Zou, *J. Phys. Chem. B* 2010, **114**, 9429.

9 (a) X. Chen, Y. Jun, K. Takanabe, K. Maeda, K. Domen, X. Z. Fu，M. Antonietti and X. Wang, Chem. Mater., 2009, **21**, 4093. (b) X. Li, J. Zhang, X. Chen, A. Fischer, A. Thomas, M. Antonietti and X. Wang, Chem. Mater., 2011, **23**, 4344.

10 (a) G. Jiang, C. Zhou, X. Xia, F. Yang, D. Tong, W. Yu and S. Liu, Mater. Lett. 2010, **64**, 2718. (b) H. Shi, G. Chen and C. Zhang, ACS Catal., 2014, **4**, 3637. (c) X. Song, X. Zhang, and P. Yang, *RSC Adv.* 2016, 6, 107433. (d) X. Song, Y. Liu, Y. Zheng, K. Ding, S. Nie, and P. Yang,, *Phys. Chem. Chem. Phys*. 2016, **18**, 4577. (e) P. Yang, X. Song, C. Jia, and H-S. Chen, *J. Indust. Eng. Chem*. 2018, **62**, 250.

11 J. Zhang, F, Guo and X. Wang, Adv. Funct. Mater., 2013, **23**, 3008.

12 (a) P. Liu, J. Y. Zhu, J. Y. Zhang, P. X. Xi, K. Tao, D. Q. Gao, D. S. Xue, ACS Energy Lett. 2017, **2**, 745. (b) J. Luxa, V. Mazanek, D. Bousa, Z. D. Sedmidubsky, M. Pumera, Z. Sofer, ChemElectroChem. 2016, **3**, 565.